Chemical Physics Letters 689 (2017) 48–55

Contents lists available at ScienceDirect

Chemical Physics Letters

journal homepage: www.elsevier.com/locate/cplett

Research paper

Modeling radical edge-site reactions of biochar in CO_2/water solution under ultrasonic treatment

Tetiana Zubatiuk [a,*], Baharak Sajjadi [b], Glake Hill [a], Danuta Leszczynska [a], Wei-Yin Chen [b], Jerzy Leszczynski [a]

[a] Interdisciplinary Center for Nanotoxicity, Jackson State University, 1400 J. R. Lynch Street, Jackson, MS 39217, USA
[b] Department of Chemical Engineering, The University of Mississippi, P.O. Box 1848, University, MS 38677, USA

ARTICLE INFO

Article history:
Received 24 June 2017
In final form 27 September 2017
Available online 28 September 2017

Keywords:
Carbon dioxide radical anion
Hydroxide radical
CO_2 capture
Biochar
Antanthrene
Electron transfer
Radical addition
Density function theory

ABSTRACT

We report results of theoretical evaluation of the mechanisms of possible radical reactions on the edge-site of biochar with $CO_2^{\cdot-}$, $\dot{O}H$, and $\dot{H}$ in irradiated aqueous solution. The computational studies were performed for model poly aromatic systems. Obtained mechanisms reflect one of the routes of the oxygen loss accompanied by increase of hydrogen content, as observed in photochemical experiment. The reaction of $CO_2^{\cdot-}$ with the edge site of biochar mainly leads to reduced rather than oxidized products. The mechanism of CO_2 capturing is mapped by different routes of one-electron reduction and radical addition to the aromatic ring.

1. Introduction

Carbon dioxide interactions with carbonaceous materials are versatile and attractive ways for the development of advanced carbon-based adsorbents for CO_2 capture. In photochemical experimental studies of Chen et al. [1] the high CO_2 uptake by biochar was observed. In the experiment, the pure CO_2 was bubbled through the aqueous mixture of biochar after which the mixture was treated with ultrasound and xenon light, at 60 °C and 1 atm conditions. After irradiation, the samples were filtered, dried and weighed. It was shown that ultrasound induces the synergistic processes: exfoliation of carbon clusters, chemisorption of CO_2 on biochar, mineral leaching, and hydrogenation. The treated biochar therefore had higher internal surface area, heating value and improved reaction rates. Small decrease in oxygen content was reflected by increase in atomic H/O and C/O ratios, which suggested that the sample was additionally highly hydrogenated. Only combined photochemical and ultrasonic treatment have been shown to induce the carbon fixation, leading to a 12.3% and 15.8% of carbon and hydrogen gain, respectively. Chen's et al. [1] work therefore demonstrated that carbon fixation through specific photochemical conditions may be a potential new route for capturing CO_2 by carbonaceous materials such as biochar.

Today, CO_2 capture and storage (CCS) is considered a crucial strategy for meeting CO_2 emission reduction targets and it is included into studies covering top research areas of catalysis [2]. The various aspects of CCS are recently reviewed and discussed by Leung et al. [3], and Aaron [4] including the state of the art technologies for CO_2 capture, separation, storage, etc. Nowadays advanced technologies, such as wet scrubber, dry regenerable sorbents, membranes, etc. have been developed and successfully used to separate the CO_2 from the flue gas [3]. The typical solid sorbents include molecular sieves, activated carbon, zeolites, calcium oxides, etc. and are used to bind the CO_2 on their surfaces [3]. The recent progresses and challenges in the syntheses of carbonaceous materials and surface functionalization for gas capture was highlighted by Gadipelli [5]. However, most of the used synthetic methods are not environmentally and economically sustainable. That is why development and application of biochar-based sorbents and functional materials has been intensively studied in recent years [6–8]. Despite several distinctions among biochar and activated carbon, from a structural viewpoint both species represent amorphous carbon with abundant porosity. However, unlike activated carbon, biochar usually has abundant surface functional groups (C—O, C═O, COOH, and OH) [7], which enhance its adsorption abilities. Li et al. [9] has reported that adsorbents with highly polarized surfaces are good for adsorption molecules with a high dipole

* Corresponding author.
E-mail address: tetiana.zubatiuk@icnanotox.org (T. Zubatiuk).

https://doi.org/10.1016/j.cplett.2017.09.058
0009-2614/

moment and the adsorbents with high electric field gradient surfaces are ideal for the adsorbate molecules characterized by high quadrupole moment. That is in agreement with experimental findings [10] that the adsorption strength of a carbonaceous materials is relatively low for H_2 and N_2; intermediate for CO, CH_4 and CO_2; and relatively high for H_2S, NH_3 and H_2O.

Since carbon dioxide is a linear molecule with a large quadrupole moment ($D_{yy} = 4.30 \times 10^{-26} esu\ cm^2$) [9] its reaction with a carbon-centered nucleophile should provide C—C coupling products, as demonstrated by trapping of carbanions by CO_2 to yield the corresponding carboxylic acids [11]. Carboxylation of carbonaceous surfaces could happen differently which is mirrored in results of various theoretical studies [12–16]. The variation in the adsorption energy, from ~3.7 eV to ~200 meV, and a broad spectrum of active binding sites, such as edge sites, pre-adsorbed alkali metals, and defects were shown in combined experimental and theoretical (B3LYP-DFT) investigations [12]. In addition to findings [5] that polar groups would enhance CO_2 capacity by strengthening adsorption and introducing additional binding sites, Wood et al. [17] found high selectivity for CO_2 adsorption with unfunctionalized, hydrogen-passivated zigzag graphitic carbon edge. In that particular case, the CO_2 binding preference was significantly higher for the edge site than for bulk graphene. This implies that higher edge concentrations could be beneficial for CO_2 capturing using nanoporous carbon [17]. The most stable complex formed by the chemisorption of CO_2 on the graphene edge sites was found to include the lactone group on the armchair edge [13]. Further dissociation of the CO_2 could occur through the formation of stable epoxy groups. Xu et al. [14] investigated the possible dissociative adsorption of CO_x on graphite surface. They reported reaction products such as oxidized graphite (epoxy groups) and a chemisorbed lactone group. However, all the reactions were found to be highly endothermic and the reaction pathways were associated with considerable energy barriers. Finally, DFT-GGA calculations [13] clearly indicated that CO_2 chemisorption can occur exothermically on the single defect of the graphite surface, after overcoming a specific energy barrier and further reaction products, such as epoxy groups, adsorbed on a renewed graphene sheet. All those findings indicate that oxygen content should increase during the adsorption of CO_2 on carbonaceous materials. Since Chen et al. [1] observed notable hydrogen gain instead of oxygen gain, it is possible that their observed products are the result of hydrogen radical reaction with the oxygen functional groups (e.g. reductive photocarboxylation) and/or radical addition of atomic hydrogen to the edge-site of aromatic sheets. The addition of atomic hydrogen to aromatics was studied by Roduner et al. [18] who demonstrated the full solvent enhancement effect for the reaction of H with benzene in water (R1) and explained it in terms of equilibrium solubility of reactants and transition state. The reductive photocarboxylation was first reported by Tazuke and Ozawa [19,20] and continuously studied. For instance, Chateauneuf et al. [21] have shown that a carbon-centered free radical could be added to CO_2 to produce a carbonyloxyl radical and then, in presence of sufficient amounts of hydrogen atom donor, carboxylic acid could be formed, (R2).

$$C_6H_6 + H^{\cdot} \rightarrow [C_6H_6 \cdots H]^{\cdot} \tag{R1}$$

$$PAH^{\cdot} + CO_2 \rightleftarrows [PAH - CO_2]^{\cdot} \overset{R-H}{\rightarrow} PAH - CO_2H. \tag{R2}$$

The experimental conditions of photochemical treatment of biochar/CO_2/H_2O system allow to assume an existence of reactive species, which could be responsible for carboxylation and hydrogenation of biochar. It is known [22], that when water is irradiated with ultrasound, the initial radical species generated are hydrated electrons, hydrogen atoms and hydroxyl radicals. The initial molecular species formed are hydrogen and hydrogen peroxide (R3). Since, CO_2 has negative reduction potential (−1.98 to −1.10 V [23]), the hydrated electrons readily add to dissolved CO_2 to form CO_2^{-} [24], (R4). The experimental study by Rosso et al. [25] has demonstrated, that CO_2^{-} easily interacts with aromatic rings, besides two reaction routes have been found: one-electron reduction (R5) and radical addition to the aromatic ring (R6).

$$H_2O \overset{\sim us}{\rightarrow} e_{aq}^{-}, H^{\cdot}, OH^{\cdot} H_2, H_2O_2, \tag{R3}$$

$$CO_2 + e_{aq}^{-} \rightarrow CO_2^{\cdot -} \tag{R4}$$

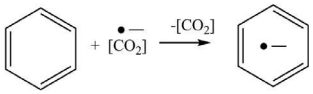

(R5)

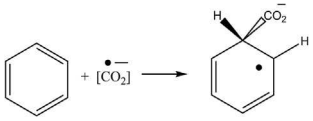

(R6)

According to known schemes [26], there are two competing reactions of $\dot{O}H$ with aromatic rings: $\dot{O}H$ radical addition to the aromatic ring to form an OH-aromatic adduct (R7) and H-atom abstraction (R8):

$$\dot{O}H + ArH \rightarrow [ArH - OH]^{\cdot}, \tag{R7}$$

$$\dot{O}H + ArH \rightarrow [Ar]^{\cdot} + H_2O. \tag{R8}$$

In order to obtain some insights into the very interesting chemistry presented in photochemical experimental studies of Chen and co-workers [1], we have performed a theoretical study of the energetics of the possible radical reactions on the aromatic edge site of biochar. And since biochar is known to contain many functional groups, the chemistry demonstrated in current study represents only a fraction of the possible products. We report on the mechanisms of one electron-transfer products formation for the reactions of $H^{\cdot}$, $OH^{\cdot}$ and $CO_2^{\cdot -}$ radicals with functionalized (—COOH, OH, C—O) and unfactionalized poly aromatic system (Fig. 1).

2. Methods

2.1. Computational details

Gaussian 09 program system [27] has been used for the quantum chemical calculations. The electronic structure of reactants, adducts, transition states, and products was calculated at the BHandHLYP/6-31G(d) level of theory under the Truhlar's et al. [28] continuum solvation model (SMD) which is recommended to account for effects of solvation [29]. SMD single-point calculations were perform based on the gas-phase geometries. BHandHLYP functional was chosen on the base of its proven effectiveness in description of radical systems [30–33]. Zang et al. [34] have shown that for electron transfer reactions the hybrid BHandHLYP method (from a large set of DFT methods, including B3LYP) is capable for predicting the structure and energetics of both the minimum energy and transition structures at a comparable accuracy with the MP2 level. Maity [30] has shown that BH and HLYP properly describes radical cation systems. Recent benchmark study of DFT methods [35] concluded that results from calculations with BHandHLYP show the best agreement with experimental data in prediction of the NMR spectra of open-shell and closed-shell molecular systems. It means that BHandHLYP functional could describe properly both geometry, relative energies and electronic properties of open-shell molecular systems.

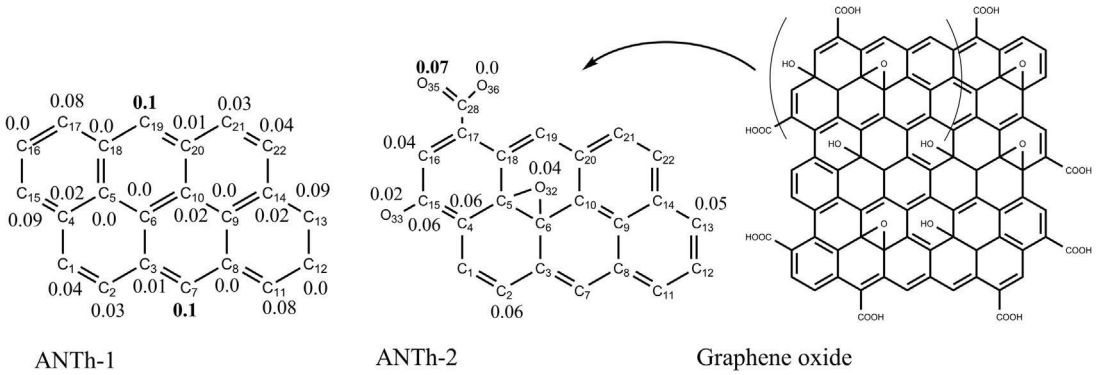

Fig. 1. The model structures of biochar, along with the Fukui indices of each atom, f_A. The missed values of f_A in ANTh-2 are the same as in ANTh-1. The edge sites of interest in the graphene oxide is shown in the parentheses (structure is adapted from Ref. [40]).

Ground-state and transition-state structures have been confirmed by frequency analyses at the same level of theory. To confirm that the transition state connects designated intermediates, intrinsic reaction coordinate calculations were performed at the same level of theory.

The studied reaction pathways are presented in the form of energy diagrams. The relative energies of the products (adducts, intermediates), which are shown on the diagrams were calculated as the energy difference between product's energy and sum of the total energies of non-interacting reagents. The total energy of reagents viz. water, CO_2^- and hydrogen atom include experimental solvation enthalpies (Table 1). ΔH_{sol} for hydroxyl radical is taken from statistical mechanics simulations [36]. The solvation enthalpy of anthanthrene molecule (ANTh) was calculated as $\Delta H_{sol} = E_{min}^{SMD} - E_{min}^{gas} + (ZPVE^{SMD} - ZPVE^{gas})$, where ZPVE is zero-point vibrational energy.

2.2. Modeling of aromatic edge site of biochar

The biochar structure that has been determined by different analytical techniques (SEM, TEM, XRD and EDX and others [7]) is mainly amorphous in nature with some local crystalline structure of highly conjugated aromatic sheets cross-linked in a random manner. The main contribution to the reactivity of biochar is the fact that the surface usually exhibits a range of hydrophilic and hydrophobic functional groups both acidic and basic [8]. Considering the high functionality and aromaticity of major part of biochar structures, the accepted structure of graphene oxide [40] (Fig. 1) was chosen as the hypothetically the closest structure appropriate to use as a model for biochar crystalline structure. We have also considered the fact, that CO_2^- radical has relatively strong dipole ($\mu_{CCSD(T)} = 0.266D$) and quadrupole ($D_{yy}^{CCSD(T)} = 6.59 \times 10^{-26} esu$) moments [41] and thus should selectively adsorbed on the edge sites of aromatic sheets which provide strong Coulombic interactions. From this point of view, the structure of basal planes could be undefined in model structure since it does not affect much the edge interactions. The edge site was taken from basic structure of graphene oxide and is represented by the substituted anthanthrene molecule, $C_{22}H_{12}$ (ANTh).

Two models have been used for simulation of radical interactions on the edge sites of biochar (Fig. 1). Since water molecule is present in mechanisms of studied reactions and strongly interacts with radical reagents, therefore one water molecule was added explicitly to the model systems. We used one unfunctionalized ANTh-1 as the reference structure. This appears to be the simplest but still adequate model for comprehensive analysis. The presence of carboxyl, hydroxyl and epoxy functional groups in ANTh-2 simulates the edge side effects at the aromatic sheets of biochar. We suggest that further extension of molecular size of model aromatic system would not change the routes of possible reactions on the active edge sites, although it could affect the energetics of those reactions. The influence of the near-parallel aromatic layers was not taken into consideration.

Table 1
Solvation enthalpy of reagents under consideration.

Reagent	ΔH_{sol}, kcal/mol	Comments
ANTh-1	−4.67	Unfunctionalized antanthrene. Current study
ANTh-2	−16.75	Functionalized with carboxyl, hydroxyl and epoxy functional group. Current study, BHandHLYP/6-31G(d)
H_2O	−10.56	Exp. value from Cox et al. (Ref. [37])
$OH^{\cdot}$	−9.38	From Monte Carlo simulations [38]. No experimental result is available
CO_2^-	−34.5	Exp. hydration energy of CO_2^- in $CO_2^- \cdot (H_2O)_4$ from Janik [24]
$H^{\cdot}$	−0.98	Solvation enthalpy of hydrogen atom usually replaced by exp. ΔH_{sol} of the hydrogen molecule [39,18]

2.3. Selection of active sites for radical attack

We used Fukui indices [42], as local reactivity descriptors, to estimate which atoms in ANTh molecule are more prone to undergo a radical attack. Although the electron density based local reactivity descriptors were proposed and successfully used decades ago [43–45], Geerlings et al. [45] demonstrated that Fukui indices could be used and are essentially important in searching the "similarity of reactivity" of a group of molecules or atoms that are similar. Recently [46] Fukui indices were successfully used to find the most probable binding sites of aromatics, which are the positions characterized by the highest density of electrons. We used the same technique and performed the natural bond orbital (NBO) population analysis [47] to obtain the condensed Fukui indices, as follows:

$$f_A^0 = 1/2[P_A(N+1) - P_A(N-1)] \quad (1)$$

where P_A stands for the population of atom A in molecule ANTh of N electrons. The NBO population analysis of the ANTh cation (N-1) and ANTh anion (N + 1) was calculated at the same equilibrium geometry as the neutral ANTh molecule to avoid the relaxation of the system. Fukui indices for each atom in ANTh are summarized in Fig. 1. The highest radical attack susceptibility is inherent to atoms C19 and C7, therefore, the reactions initiated by radicals most preferentially occur at these positions, producing ANTh adducts (e.g. R1-2, R5-8). The predicted activity of centered atoms

on the edge site of anthanthrene is in line with computational studies for naphthalene [48] and anthracene [33]. The functional groups do not lower the radical attack susceptibility of C19 and C7, but they influence the activity of new sites. The presence of hydroxy, epoxy and carboxyl groups in ANTh-2 strengthens the susceptibility for radical attack for sites C2, C4, and C16. Unlike oxygens of epoxy and hydroxy groups, the carboxylic oxygen O35 in ANTh-2 is expected to become an additional active site for radical attack due to higher Fukui index (Fig. 1).

3. Results and discussion

3.1. Hydrogen radical and hydroxyl radical attacks

Before considering the details of the reactions on the C19 active site, we tested the relative stabilities of the $\dot{O}H$ adducts with less active C21 site. The Fukui indexes for C19 and C21 are 0.1 and 0.03, respectively (Fig. 1). The adducts [C_{19}-OH, C_{19}-H] and [C_{21}-OH, C_{21}-H] are formed by the $\dot{O}H$ addition to ANTh-1 without loss of H atom (R9). According to computed enthalpy change, ΔH the reaction of $\dot{O}H$ radicals with ANTh-1 is exothermic and barrierless; obtained low activation energies: ΔE_a (a) = −0.2 kcal/mol and (b) 0.7 kcal/mol) are consistent with the experimental findings of Ananthula et al. [49], in which the activation energy is negative −1.08 kcal/mol [373–498 K] for OH radical addition to PAH. The addition of the $\dot{O}H$ radical to C19 site is favored by only 10 kcal/mol over the addition to C21, which indicates that same radical additions could happen on the less active edge carbons along the aromatic sheets of biochar. Both adducts are open-shell species and will likely react with another radicals or loose OH, or loose H atom bonded to the same carbon [48].

We have found that H-atom abstraction by free OH radical is less favorable and is associated with notable energy barrier (Table 2, *c*). This is in accordance with experimental rates obtained by Ananthula et al. [49], indicating that mechanism of OH radical reaction with multiple ring PAH is dominated by OH addition with H abstraction being a minor contributor.

When the [C_{19}-OH, C_{19}-H] adduct is formed, there are several possible reactions: (i) the loss of the $\dot{O}H$, (ii) the loss of H1 atom bonded to the same carbon as the OH group and subsequent (iii) shift of the H1 to the adjacent carbon atom C21. Process (i) is the reverse to the formation step. Based on the reaction barriers (Table 2, d, *e*) the loss of $\dot{O}H$ is about 12 kcal/mol more favorable than $\dot{H}$ desorption (ii) from the same carbon site. Both processes are highly endoenergetic. As found, the 19,21 H shift (iii) to convert the alcohol [C_{19}-OH, C_{19}-H] to the ketone [C_{19}-O, C_{21}-H,H] has a barrier of about 55 kcal/mol (Table 2, *d*). Thus, H hydrogen transfer to adjacent site C21 seems unfavorable. However, addition of H atom to C21 site can occur because of presence of free H atoms in irradiated solution. Addition of H atom to carbon sites is highly exoenergetic and has low activation energy (Table 2, *f, g*). As shown in Fig. 2 formation of carbonyl group [C_{19}-O, C_{21}-H,H] is less favorable than formation of hydroxy group [C_{19}-OH, C_{21}-H,H], additionally carbonyl group is readily hydrogenated with about 65 kcal/mol gain in system energy (Table 2, *h*). Based on reactions energetics (Table 2, Fig. 2), we conclude that reaction of OH with ANTh-1 leads mostly to formation of the [C_{19}-OH, C_{19}-H] and/or [C_{21}-OH, C_{21}-H]. We are unable to definitely determine if the addition of OH is reversible or not, but we found that the loss of OH is easier than loss of H atom. Since hydrogenation is highly favorable process, then in couple with preferable loss of OH, it explains why the notable increase in hydrogen content rather than in oxygen content was observed in the experiment with the treated biochar [1].

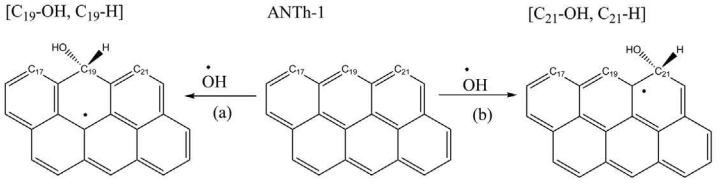

(a) ΔH = -43.2 kcal/mol, Ea = -0.2 kcal/mol (b) ΔH = -35.3 kcal/mol, Ea = 0.7 kcal/mol

(R9)

Further, we discuss the one electron-transfer mechanisms for radical addition of $CO_2^{\cdot-}$, $\dot{O}H$ and $\dot{H}$ to C19 active site. The overall reaction energetics are summarized in Fig. 2 and are given in Table 2. Similar to OH barrierless addition (<1 kcal/mol), reaction of H with C19 site occurs with a small barrier of 3.8 kcal/mol and notable gain in energy (Table 1, *a*). Obtained activation energy is in line with experimental findings by Roduner et al. [18], who measured the rate constants for the addition of H atoms to benzene as a function of temperature in aqueous solution and reported average Arrhenius activation energy, E_a = 19.1(6) kJ/mol (4.6 kcal/mol). According to reaction pathways from Fig. 2, first, $\dot{O}H$ radical and ANTh-1 form a pre-reaction complex [PRC] by means of intermolecular hydrogen bonding of 2.28 Å between $\dot{O}H$ and C19 and 1.53 Å between $\dot{O}H$ and water molecule. This is parallel with about 14 kcal/mol gain in the system energy from the desolvation of reacting species. The transition state TS1 lies below of energy minimum of non-interacting reagents, hence $\dot{O}H$ radical addition happens barrierless (with negative activation energy, Table 2, *b*). The one-electron transfer reaction is exoenergetic by −43.2 kcal/mol.

3.2. Carbon dioxide anion radical attack

The overall reaction energetics are summarized in Figs. 3,4 and are given in Table 3. Like the $\dot{O}H$ radical, the $\dot{C}O_2^-$ and ANTh-1 form first a pre-reaction complex [PRC] by means of intermolecular π-π interaction (3.55 Å) between C19 and carbon atom of $CO_2^{\cdot-}$ with notable energy gain from the desolvation. In [PRC] the extra spin density is preserved at the carbon of $CO_2^{\cdot-}$ (0.72 electrons). Since transition state TS1 lies below the energy minimum of non-interacting reagents, then $\dot{C}O_2^-$ radical addition to aromatic ring happens barrierless (with negative activation energy, Table 3, *a*). In radical adduct [C_{19}-CO_2, C_{19}-H] the highest electron density was found at carbon C7 (0.5 electrons), while the electron density at carbon of —COO group became 0.03 electrons. The partially negative charge in radical adduct is located on the carboxylic group (−0.73 electrons).

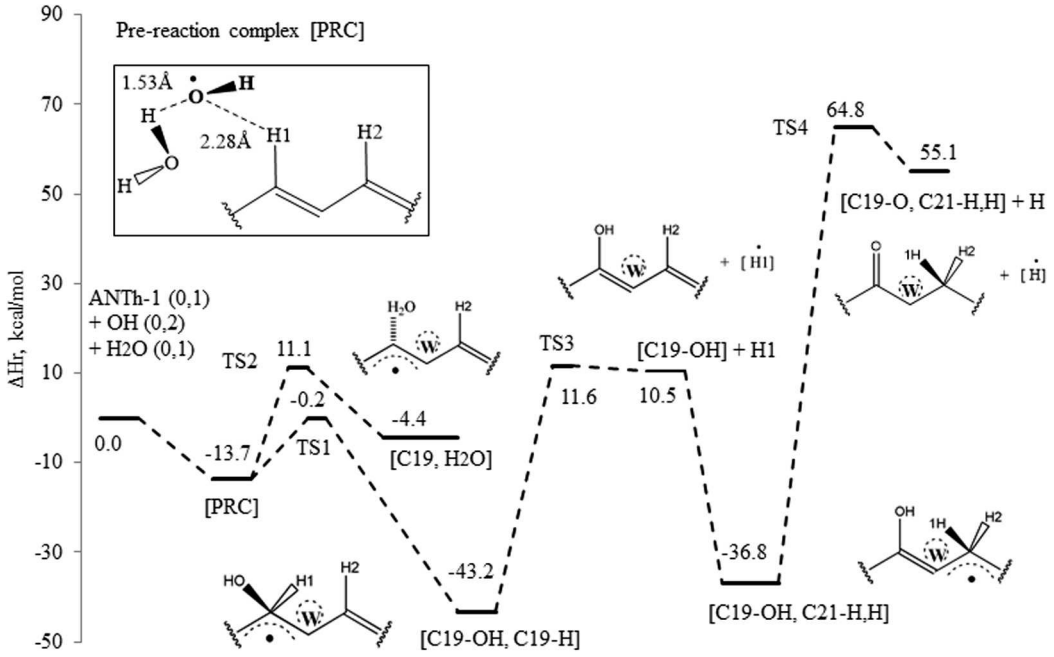

Fig. 2. The reaction profiles for the one-electron transfer reactions of $\dot{H}$ and $\dot{OH}$ radicals and ANTh-1 in aqueous solution. The explicit water molecule is marked as "W". 0.0 kcal/mol on the relative energy axis corresponds to the sum of energies of non-interacting reagents: ANTh-1, $\dot{O}H$, H_2O.

Table 2
Heat of reaction (ΔH_r) and activation energy (ΔE_a) for the reactions of $\dot{H}$ and $\dot{OH}$ radicals with unfactionalized ANTh-1 in aqueous solution.

	Radical reactions	ΔE_a, kcal/mol	ΔH_r, kcal/mol
a	ANTh-1 + $H^{\cdot}$ → [C_{19}-H, C_{19}-H]$^{\cdot}$	3.8	−65.4
b	ANTh-1 + $OH^{\cdot}$ → [C_{19}-OH, C_{19}-H]$^{\cdot}$	−0.2	−43.2
c	ANTh-1 + $OH^{\cdot}$ → [C_{19}]$^{\cdot}$…H_2O	11.1	−4.4
d	[C_{19}-OH, C_{19}-H]$^{\cdot}$ → [C_{19}-OH]…$H^{\cdot}$	54.8	53.7
e	[C_{19}-OH, C_{19}-H]$^{\cdot}$ → [C_{19}-H]…$OH^{\cdot}$	43.0	29.5
f	[C_{19}-OH]…$H^{\cdot}$ → [C_{19}-OH, C_{19}-H]$^{\cdot}$	1.1	−53.7
g	[C_{19}-OH]…$H^{\cdot}$ → [C_{19}-OH, C_{21}-H,H]$^{\cdot}$	−2.4	−47.3
h	[C_{19}-O, C_{21}-H,H]…$H^{\cdot}$ → [C_{19}-OH, C_{21}-H,H]$^{\cdot}$	9.7	−91.9
i	[C_{19}-OH, C_{21}-H,H]$^{\cdot}$ → [C_{19}-O, C_{21}-H,H]…$H^{\cdot}$	101.6	91.9

After the [C_{19}-CO_2, C_{19}-H] is formed, there are several possible reactions (Fig. 3): (i) loss of H atom, bonded to the same carbon as CO_2 group, and formation of carboxylic acid; (ii) interaction with water molecule and formation of intermediate of cyclohexadienyl radical derivative [C_{19}-H, C_{19}-H], Reaction (R10); (iii) interaction with water and formation of hydrohycyclohexadienyl radical derivative [C_{19}-OH, C_{19}-H], (R11, a); (iv) alternatively, the CO_2-adduct could be converted to the alcohol [C_{19}-OH, C_{19}-H] by the elimination of high energized $H\dot{O}CO$ radical, (R11, b). For the corresponded products of the (iv) reaction the sum of atomic spin densities is greater (0.98 vs 0.02) at $H\dot{O}CO$ and the negative charge (−0.92 vs −0.08) is distributed over the aromatic molecule, thus indicating formation of closed-shell [C_{19}-OH, C_{19}-H] anion. Desorption of radical species as H atom (i) and $H\dot{O}CO$ (iv) is associated with considerable energy barriers, (Table 3, *b, e*), which are higher than desorption of $CO_2^{\cdot-}$ by 27 kcal/mol and 43 kcal/mol respectively. Thus, proposed mechanisms do not show formation of carbonic acid or alcohol as preferable products of $CO_2^{\cdot-}$ oxidation. More likely, radical carboxylation occurs in more complicated way, different from the simple addition of $CO_2^{\cdot-}$ to aromatic ring. For instance, the reaction pathways in Fig. 3 demonstrate that free $H\dot{O}CO$ easily interact with alcohols [C_{19}-OH] to form CO_2-adduct. This reaction is highly exoenergetic and has low activation energy (Table 3, *f*). Free$H\dot{O}CO$ radicals could appear in aqueous solution by $CO_2^{\cdot-}$ protonation: $CO_2^{\cdot-} + H^+ \leftrightarrow H\dot{O}CO$ [24].

The experimental study of Janik [24] has revealed that $CO_2^{\cdot-}$ interacts very strongly with water, but exists as a distinct chemical species and that water molecules stabilize the excess electron. However, as could be seen from Fig. 3 in presence of ANTh molecule $CO_2^{\cdot-}$ easily oxidizes and forms the hydrocarbonate anion with the gain of about 10 kcal/mol in system energy (Table 3, c). It is interesting to note, that the heat of reaction for $[HCO_3]^-$ formation is nearly two times higher than for $[HCO_2]^-$ formation, as it is expected for the better leaving group HCO_3^- than HCO_2^- (Table 3, *c, d*); this is because H_2CO_3 is weaker base (pKa = 6.37) than H_2CO_2 (pKa = 3.75). Based on the results of these calculations, we conclude that radical carboxylation in solution is highly favorable, however subsequent H atom desorption and formation of carboxylic acid is associated with high barrier. Interaction with water molecules is unlikely to provide the alcohol or cyclohexadienyl radical products in high yield because of high activation barriers. The predicted reaction pathway with $H\dot{O}CO$ radical demonstrates the alternative route of carboxylation of biochar edge-site in which hydroxyl groups are transformed to carboxylic ones.

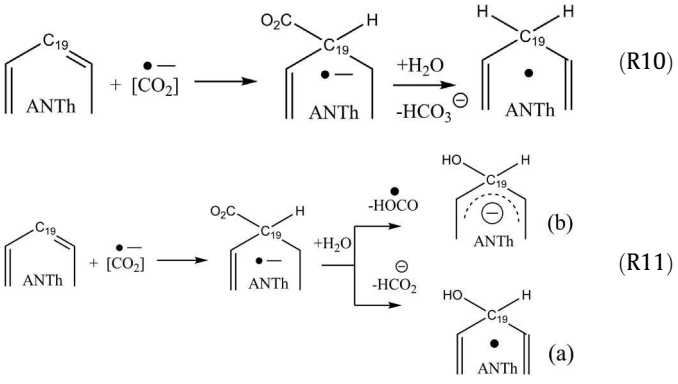

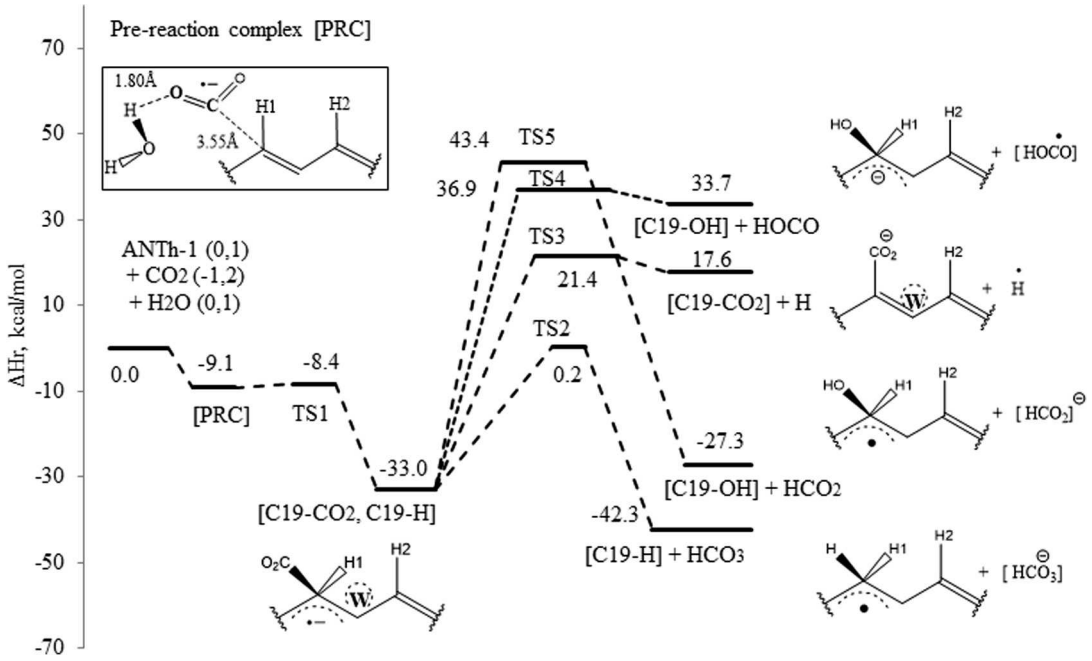

Fig. 3. The reaction profiles for the reactions of $\dot{C}O_2^-$ with ANTh-1 in aqueous solution. The explicit water molecule is marked as "W". 0.0 kcal/mol on the relative energy axis corresponds to the sum of energies of non-interacting reagents: ANTh-1, $\dot{C}O_2^-$, H_2O.

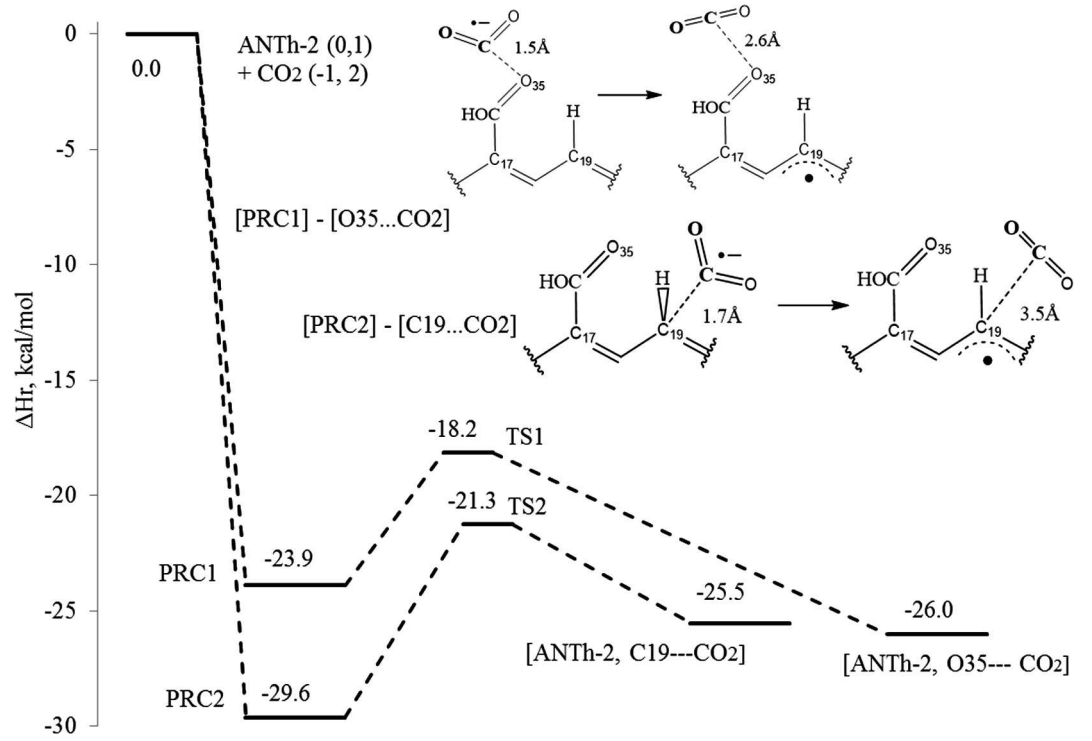

Fig. 4. The reaction profiles for the reactions of $\dot{C}O_2^-$ with ANTh-2 in aqueous solution. 0.0 kcal/mol on the relative energy axis corresponds to the sum of energies of non-interacting reagents: ANTh-2, $\dot{C}O_2^-$.

We have studied two reaction pathways with functionalized ANTh-2 and have shown two alternative routes for CO_2^- radical oxidation: with oxygen O35 of carboxylic group and with C19 of aromatic ring (Fig. 4). Similarly to previous mechanisms obtained for $\dot{C}O_2^-$ radical attack, formation of pre-reaction complexes with appearance of $\dot{C}O_2^-$ either near the O35 site [O35...CO_2] or C19 site [C19...CO_2] is highly favorable and occurs with about 30 kcal/mol gain of energy due to the desolvation of reacting spices (Table 3, *h*, *i*). The structures of [PRC] are shown in Fig. 4. In contrast to barrierless $\dot{C}O_2^-$ radical addition to the aromatic ring (Fig. 3), one-electron reduction (Fig. 4) occurs with a barrier of about 6–8 kcal/mol depending on the site of reduction (Table 3, *j*, *k*). The electron

Table 3
Heat of reaction (ΔH_r) and activation energy (ΔE_a) for the reactions of $\dot{C}O_2^-$ radical with ANTh-1 and ANTh-2 in aqueous solution.

	Radical reactions	ΔE_a, kcal/mol	ΔH_r, kcal/mol
a	ANTh-1 + $\dot{C}O_2^-$ → $[C_{19}\text{-}CO_2, C_{19}\text{-}H]^{\cdot -}$	−5.8	−32.8
b	$[C_{19}\text{-}CO_2, C_{19}\text{-}H]^{\cdot -}$ → $[C_{19}\text{-}CO_2]^- + H^{\cdot}$	54.5	50.6
c	$[C_{19}\text{-}CO_2, C_{19}\text{-}H]^{\cdot -} + H_2O$ → $[C_{19}\text{-}H]^{\cdot} + HCO_3^-$	33.2	−9.3
d	$[C_{19}\text{-}CO_2, C_{19}\text{-}H]^{\cdot -} + H_2O$ → $[C_{19}\text{-}OH]^{\cdot} + HCO_2^-$	76.4	5.7
e	$[C_{19}\text{-}CO_2, C_{19}\text{-}H]^{\cdot -} + H_2O$ → $[C_{19}\text{-}OH]^- + HOCO^{\cdot}$	69.9	66.7
f	$[C_{19}\text{-}OH]^{\cdot} + HOCO^{\cdot}$ → $[C_{19}\text{-}CO_2, C_{19}\text{-}H]^{\cdot -} + H_2O$	3.2	−66.7
g	$[C_{19}\text{-}OH]^{\cdot} + H^{\cdot}$ → $[C_{19}\text{-}CO_2, C_{19}\text{-}H]^{\cdot -}$	3.8	−50.6
h	ANTh-2 + $\dot{C}O_2^-$ → $[C_{19}\text{-}CO_2]^{\cdot -}$	–	−29.6
i	ANTh-2 + $\dot{C}O_2^-$ → $[O_{35}\text{-}CO_2]^{\cdot -}$	–	−23.9
j	$[C_{19}\text{-}CO_2]^{\cdot -}$ → $[\text{ANTh-2}]^{\cdot -} + CO_2$	8.3	4.1
k	$[O_{35}\text{-}CO_2]^{\cdot -}$ → $[\text{ANTh-2}]^{\cdot -} + CO_2$	5.7	−2.1

transfer from $\dot{C}O_2^-$ radical to either carboxyl group or aromatic ring yield the same [ANTh-2] radical anion (R12) with the same spin-density distribution over the aromatic system. The high active radical of ANTh can subsequently attach hydrated electrons from irradiated solution and become the neutral product and/or according to Chateauneuf [21] – attach CO_2 to produce a carboxylic acid in excess of hydrogen atom donors (R1).

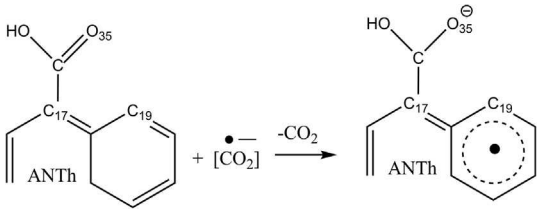

(R12)

4. Summary

In this work, the radical reactions mechanisms of edge-site of biochar with $\dot{C}O_2^-$, $\dot{O}H$, and $\dot{H}$ in irradiated aqueous solution is predicted by application of reliable computational methods and discussed in detail. The computational studies were performed using model poly aromatic systems to explain the results of experimental work of Chen et al. [1]. We have found that addition of radicals $\dot{C}O_2^-$, $\dot{O}H$, and $\dot{H}$ is highly favorable and occurs with notable gain in system energy. This indicates that edge site of biochar immediately restores under ultrasonic treatment of aqueous mixture of biochar and carbon dioxide. For the OH-adduct, the preferable subsequent path is the loss of the OH, and the next favorable option is the loss of an H atom to form the alcohol and then ketone. Since, first, the loss of OH has lower barrier than the loss of H atom, bonded to the same site and, second, H atom easily adds to the carbon sites with oxygen functional groups (—OH, —COOH and —C═O), we could conclude that addition of $\dot{O}H$ and $\dot{H}$ likely produces hydrogen-rich, rather than oxygen-rich products. Moreover, the hydroxyl and carbonyl groups, which are presented in the structure of biochar could be easily replaced by the addition of H atoms. This mechanism reflects one of the possible routes of oxygen loss and notable increase of hydrogen content which were found for photochemically treated biochar. The increase of carbon content in treated biochar is explained by different routes of radical carboxylation. In the first instance, it is barrierless radical addition of $\dot{C}O_2^-$ to the aromatic rings. The last reaction competes with the interaction of free $\dot{C}O_2^-$ with water, which leads to formation of stable $[HCO_3]^-$ anion. The desorption of CO_2 group through the interaction with water molecule is unlikely to occur because of high activation barriers of corresponded reactions. Second, the revealed here reaction pathway with $H\dot{O}CO$ radical demonstrates the alternative route of carboxylation of biochar edge-site in which hydroxyl groups are transformed to carboxylic groups. Third, one-electron reduction of the aromatic ring by $\dot{C}O_2^-$ leads to formation of highly active radical aromatic ring which can subsequently attach hydrated electron, hydrogen or hydroxyl radical from irradiated solution, or attach CO_2 to produce a carboxylic acid. The last option reflects the alternative pathway of reductive carboxylation in presence of sufficient amounts of hydrogen atom donor.

Acknowledgements

This work was supported by NSF EPSCoR RII Grant No. OIA-1632899. We thank the Mississippi Center for Supercomputer Research (Oxford, MS, USA) for an allotment of computer time. The authors acknowledge the Extreme Science and Engineering Discovery Environment (XSEDE) award DMR100088, which is supported by National Science Foundation Grant Number ACI-1053575.

References

[1] W.-Y. Chen, D.L. Mattern, J.C.S. Eneruvie Okinedo, A.A. Mattei, C.W. Redwine, Photochemical and acoustic interactions of biochar with CO_2 and H_2O: applications in power generation and CO2 capture, AIChE J. 60 (3) (2014) 1054–1065.
[2] M.L. Bell et al., Climate change, ambient ozone, and health in 50 US cities, Clim. Change 82 (1–2) (Mar. 2007) 61–76.
[3] D.Y.C. Leung, G. Caramanna, M.M. Maroto-Valer, An overview of current status of carbon dioxide capture and storage technologies, Renew. Sustain. Energy Rev. 39 (Nov. 2014) 426–443.
[4] D. Aaron, C. Tsouris, Separation of CO_2 from flue gas: a review, Sep. Sci. Technol. 40 (1–3) (Jan. 2005) 321–348.
[5] S. Gadipelli, Z.X. Guo, Graphene-based materials: synthesis and gas sorption, storage and separation, Prog. Mater. Sci. 69 (Apr. 2015) 1–60.
[6] A.E. Creamer, B. Gao, M. Zhang, Carbon dioxide capture using biochar produced from sugarcane bagasse and hickory wood, Chem. Eng. J. 249 (2014) 174–179.
[7] W.-J. Liu, H. Jiang, H.-Q. Yu, Development of biochar-based functional materials: toward a sustainable platform carbon material, Chem. Rev. 115 (22) (Nov. 2015) 12251–12285.
[8] J. Lehmann, S. Joseph, Biochar for environmental management: An Introduction, in: J. Lehmann, S. Joseph (Eds.), Biochar for Environmental Management: Science and Technology, Earthscan, London, 2009, pp. 1–10.
[9] J.-R. Li, R.J. Kuppler, H.-C. Zhou, Selective gas adsorption and separation in metal–organic frameworks, Chem. Soc. Rev. 38 (5) (2009) 1477.
[10] R.T. Yang, Adsorbents: Fundamentals and Applications, John Wiley & Sons Inc, Hoboken, NJ, USA, 2003.
[11] M. Aresta, A. Dibenedetto, E. Quaranta, Reaction Mechanisms in Carbon Dioxide Conversion, Springer, Berlin Heidelberg, Berlin, Heidelberg, 2016.
[12] A. Montoya, F. Mondragón, T.N. Truong, CO_2 adsorption on carbonaceous surfaces: a combined experimental and theoretical study, Carbon N. Y. 41 (1) (Jan. 2003) 29–39.
[13] P. Cabrera-Sanfelix, Adsorption and reactivity of CO_2 on defective graphene sheets, J. Phys. Chem. A 113 (2) (Jan. 2009) 493–498.
[14] S.C. Xu, S. Irle, D.G. Musaev, M.C. Lin, Quantum chemical prediction of reaction pathways and rate constants for dissociative adsorption of COx and NOx on the graphite (0001) surface, J. Phys. Chem. B 110 (42) (Oct. 2006) 21135–21144.
[15] A. Allouche, Y. Ferro, Dissociative adsorption of small molecules at vacancies on the graphite (0001) surface, Carbon N.Y. 44 (15) (Dec. 2006) 3320–3327.
[16] J. Jiang, S.I. Sandler, Separation of CO_2 and N_2 by Adsorption in C_{168} Schwarzite: a combination of quantum mechanics and molecular simulation study, J. Am. Chem. Soc. 127 (34) (Aug. 2005) 11989–11997.
[17] B.C. Wood et al., Methane and carbon dioxide adsorption on edge-functionalized graphene: a comparative DFT study, J. Chem. Phys. 137 (5) (Aug. 2012) 54702.
[18] E. Roduner, D.M. Bartels, Solvent and isotope effects on addition of atomic hydrogen to benzene in aqueous solution, Ber. Bunsenges. Phys. Chem. 96 (8) (1992) 1037–1042.
[19] S. Tazuke, H. Ozawa, Photofixation of carbon dioxide: formation of 9,10-dihydrophenanthrene-9-carboxylic acid from phenanthrene_amine_carbon dioxide systems, J. Chem. Soc. Chem. Commun (1975) 237–238.
[20] S. Tazuke, S. Kazama, N. Kitamura, Reductive photocarboxylation of aromatic hydrocarbons, J. Org. Chem. 51 (1986) 4548–4553.
[21] J.E. Chateauneuf, J. Zhang, J. Foote, J. Brink, M.W. Perkovic, Photochemical fixation of supercritical carbon dioxide: the production of a carboxylic acid from a polyaromatic hydrocarbon, Adv. Environ. Res. 6 (4) (Oct. 2002) 487–493.
[22] P. Riesz, D. Berdahl, C.L. Christman, Fundamental World of Quantum Chemistry, Springer, Netherlands, Dordrecht, 2004.

[23] W.H. Koppenol, J.D. Rush, Reduction potential of the carbon dioxide/carbon dioxide radical anion: a comparison with other C1 radicals, J. Phys. Chem. 91 (16) (Jul. 1987) 4429–4430.
[24] I. Janik, G.N.R. Tripathi, The nature of the CO_2 − radical anion in water, J. Chem. Phys. 144 (15) (Apr. 2016) 154307.
[25] J.A. Rosso, S.G. Bertolotti, A.M. Braun, D.O. Mártire, M.C. Gonzalez, Reactions of carbon dioxide radical anion with substituted benzenes, J. Phys. Org. Chem. 14 (5) (May 2001) 300–309.
[26] F. Goulay, C. Rebrion-Rowe, J.L. Le Garrec, S.D. Le Picard, A. Canosa, B.R. Rowe, The reaction of anthracene with OH radicals: an experimental study of the kinetics between 58 and 470K, J. Chem. Phys. 122 (10) (Mar. 2005) 104308.
[27] M.J. Frisch et al., Gaussian 09, Revision D.01, Gaussian, Inc., Wallingford CT. 2009.
[28] A.V. Marenich, C.J. Cramer, D.G. Truhlar, Universal solvation model based on solute electron density and on a continuum model of the solvent defined by the bulk dielectric constant and atomic surface tensions, J. Phys. Chem. B 113 (18) (May 2009) 6378–6396.
[29] F. Weinhold, C.R. Landis, Natural bond orbitals and extensions of localized bonding concepts, Chem. Educ. Res. Pr. 2 (2) (Nov. 2001) 91–104.
[30] D.K. Maity, Structure, bonding, and spectra of cyclic dithia radical cations: a theoretical study, J. Am. Chem. Soc. 124 (28) (Jul. 2002) 8321–8328.
[31] J.R. Alvarez-Idaboy, A. Galano, G. Bravo-Pérez, M.E. Ruiz, Rate constant dependence on the size of aldehydes in the NO_3 + aldehydes reaction. an explanation via quantum chemical calculations and CTST, J. Am. Chem. Soc. 123 (34) (Aug. 2001) 8387–8395.
[32] W.-J. Ding, D.-C. Fang, Theoretical studies on cycloaddition reactions between keteniminium cations and olefins, J. Org. Chem. 66 (20) (Oct. 2001) 6673–6678.
[33] D. Wang, Y. Li, M. Yang, M. Han, Decomposition of polycyclic aromatic hydrocarbons in atmospheric aqueous droplets through sulfate anion radicals: an experimental and theoretical study, Sci. Total Environ. 393 (1) (Apr. 2008) 64–71.
[34] Q. Zhang, R. Bell, T.N. Truong, Ab initio and density functional theory studies of proton transfer reactions in multiple hydrogen bond systems, J. Phys. Chem. 99 (2) (1995) 592–599.
[35] J. Wu, Z. Chai, D. Wang, A benchmark study of DFT methods on the electronic properties of lanthanofullerenes: a case study of Ce@C2v(9)-C82 anion, RSC Adv. 3 (48) (2013) 26252.
[36] P. Cabral do Couto, R.C. Guedes, B.J. Costa Cabral, J.A. Martinho Simões, The hydration of the OH radical: microsolvation modeling and statistical mechanics simulation, J. Chem. Phys. 119 (14) (Oct. 2003) 7344–7355.
[37] J.D. Cox, D.D. Wagman, V.A. Medvedev (Eds.), CODATA Key Values for Thermodynamics, Hemisphere, New York, 1989.
[38] P. Cabral do Couto, R.C. Guedes, B.J. Costa Cabral, J.A. Martinho Simões, The hydration of the OH radical: microsolvation modeling and statistical mechanics simulation, J. Chem. Phys. 119 (14) (Oct. 2003) 7344–7355.
[39] E.J. Brändas, E.S. Kryachko (Eds.), Fundamental World of Quantum Chemistry, Springer, Netherlands, Dordrecht, 2004.
[40] D.R. Dreyer, S. Park, C.W. Bielawski, R.S. Ruoff, The chemistry of graphene oxide, Chem. Soc. Rev. 39 (1) (2010) 228–240.
[41] G.L. Gutsev, R.J. Bartlett, R.N. Compton, Electron affinities of CO_2, OCS, and CS2, J. Chem. Phys. 108 (16) (Apr. 1998) 6756–6762.
[42] F. Jensen, Introduction to Computational Chemistry, Wiley, Chichester, 2007.
[43] R.K. Roy, S. Krishnamurti, P. Geerlings, S. Pal, Local softness and hardness based reactivity descriptors for predicting intra- and intermolecular reactivity sequences: carbonyl compounds, J. Phys. Chem. A 102 (21) (May 1998) 3746–3755.
[44] F. Gilardoni, J. Weber, H. Chermette, T.R. Ward, Reactivity indices in density functional theory: a new evaluation of the condensed Fukui function by numerical integration, J. Phys. Chem. A 102 (1998) 3607–3613.
[45] P. Geerlings, G. Boon, C. Van Alsenoy, F. De Proft, Density functional theory and quantum similarity, Int. J. Quantum Chem. 101 (6) (2005) 722–732.
[46] I.J. Bazany-Rodríguez, D. Martínez-Otero, J. Barroso-Flores, A.K. Yatsimirsky, A. Dorazco-González, Sensitive water-soluble fluorescent chemosensor for chloride based on a bisquinolinium pyridine-dicarboxamide compound, Sens. Actuat. B Chem. 221 (Dec. 2015) 1348–1355.
[47] F. Weinhold, C.R. Landis, Natural bond orbitals and extension of localized bonding concepts, Chem. Educ. Res. Pr. 2 (2) (2001) 91–104.
[48] A. Ricca, C.W. Bauschlicher Jr, The reactions of polycyclic aromatic hydrocarbons with OH, Chem. Phys. Lett. 328 (4–6) (Oct. 2000) 396–402.
[49] R. Ananthula, T. Yamada, P.H. Taylor, Kinetics of OH radical reaction with anthracene and anthracene- d 10, J. Phys. Chem. A 110 (10) (Mar. 2006) 3559–3566.